1874–1888 *Nucleic Acids Research, 2010, Vol. 38, No. 6* *Published online 30 December 2009*
doi:10.1093/nar/gkp1153

RepD-mediated recruitment of PcrA helicase at the *Staphylococcus aureus* pC221 plasmid replication origin, *oriD*

C. Machón[1], G. P. Lynch[2], N. H. Thomson[2], D. J. Scott[3], C. D. Thomas[2] and P. Soultanas[1,*]

[1]Centre for Biomolecular Sciences, School of Chemistry, University of Nottingham University Park, Nottingham NG7 2RD, [2]Astbury Centre for Structural Molecular Biology, University of Leeds, Leeds LS2 9JT and [3]National Centre for Molecular Hydrodynamics, School of Biosciences, University of Nottingham, Sutton Bonington, Leics LE12 5RD, UK

Received August 28, 2009; Revised November 6, 2009; Accepted November 23, 2009

ABSTRACT

Plasmid encoded replication initiation (Rep) proteins recruit host helicases to plasmid replication origins. Previously, we showed that RepD recruits directionally the PcrA helicase to the pC221 *oriD*, remains associated with it, and increases its processivity during plasmid unwinding. Here we show that RepD forms a complex extending upstream and downstream of the core *oriD*. Binding of RepD causes remodelling of a region upstream from the core *oriD* forming a 'landing pad' for the PcrA. PcrA is recruited by this extended RepD–DNA complex via an interaction with RepD at this upstream site. PcrA appears to have weak affinity for this region even in the absence of RepD. Upon binding of ADPNP (non-hydrolysable analogue of ATP), by PcrA, a conformational rearrangement of the RepD–PcrA–ATP initiation complex confines it strictly within the boundaries of the core *oriD*. We conclude that RepD-mediated recruitment of PcrA at *oriD* is a three step process. First, an extended RepD–*oriD* complex includes a region upstream from the core *oriD*; second, the PcrA is recruited to this upstream region and thirdly upon ATP-binding PcrA relocates within the core *oriD*.

INTRODUCTION

R-plasmids encode antimicrobial resistance genes that are a major cause for spread and establishment of antimicrobial resistance in bacteria. The *Staphylococcus aureus* plasmid pC221 is a 4.6 kb multi-copy plasmid carrying a gene conferring resistance to chloramphenicol (Cm^r). Together with pC223 and pC194 they constitute the prototype Cm^r plasmids in this organism (1). The spread of antibiotic resistance among *S. aureus* is not confined to chloramphenicol. Plasmid mediated resistance is also found for other antibiotics such as amoxicillin and tetracycline in a high proportion of clinical isolates (2). These Cm^r plasmids replicate via rolling circle plasmid replication. Initiation of replication is mediated by plasmid encoded replication initiation proteins known as Rep proteins (3–5). Rep proteins exhibit topoisomerase I activity, bind to their cognate plasmid origins of replication, nick one strand (known as the (+) strand) and attach themselves covalently at the 5′-end of the nick via a phosphotyrosine bond utilizing an essential active site tyrosine residue (6–8). They recruit a host helicase at the origin and the Rep–helicase complex then facilitates directional unwinding of the duplex DNA during rolling-circle plasmid replication (9,10).

The pC221 plasmid encodes a dimeric RepD protein (37.5 kDa) that initiates replication from its cognate *oriD* (7) by recruiting the host PcrA helicase and stimulating its activity (10–12). PcrA is an essential enzyme found in all Gram positive bacteria. It is homologous to the UvrD and Rep helicases of Gram negative bacteria and is involved in DNA repair, and the resolution of stalled replication forks and RecFOR-mediated blocked recombination structures (13,14). Its role in rolling-circle plasmid replication was identified genetically. A *pcrA3* mutation in *S. aureus* resulted in accumulation of plasmid replication initiation complexes and a consequent reduction in plasmid copy number of pT181-related plasmids (15–17). The acronym PcrA (plasmid copy number reduction) reflects its important role in plasmid replication. Functional, genetic and direct interactions between PcrA and Rep proteins have been established. For example, suppressor mutations alleviating the effect of the *pcrA3* mutation were identified and mapped in the pT181-encoded *repC* gene (17).

*To whom correspondence should be addressed. Tel: +44 0 1159513525; Fax: +44 0 1158468002; Email: panos.soultanas@nottingham.ac.uk

The *pcrA3* mutation was mapped as T61I within the PcrA3 protein (18). *Staphylococcus aureus* PcrA functionally interacted with RepC to mediate pT181 plasmid unwinding (19). The *Bacillus cereus* and *B. anthracis* PcrA helicases were able to interact with RepC and support the replication of the *S. aureus* pT181 plasmid (20), the *Streptococcus pneumoniae* PcrA supported RepC-mediated unwinding of the *S. aureus* pT181 plasmid (21), whereas the *B. stearothermophilus* PcrA was able to interact with RepD (encoded by *S. aureus* pC221 plasmid) and completely unwind an *oriD*-containing plasmid in the presence of SSB (10). Direct interactions between Rep and PcrA proteins so far have been detected by pull down assays followed by western blotting using MBP-tagged Rep proteins and anti-MBP antibodies (18–20). These data show that Rep proteins can interact with heterologous PcrA helicases, a property that may have contributed to the ability of rolling-circle replication plasmids to disseminate and propagate in a broad range of Gram positive hosts.

The molecular events of Rep-mediated recruitment of helicases at plasmid replication origins are poorly understood. The pC221 *oriD* consists of three inverted complementary repeats, ICR I-III (7). RepD covalently attaches at the 5′-end of a nick in the middle of ICR II (7) and participates in the directional recruitment of PcrA (10) and to increase its processivity (10,11), but the molecular details of their interactions at *oriD* during loading are not known. In an effort to understand this better, we carried out systematic exonuclease III (ExoIII) footprinting and direct imaging by atomic force microscopy (AFM) of the pC221 *oriD* in the presence and absence of RepD, PcrA and nucleotides. Our data suggest that binding of RepD to *oriD* forms an extended structure encompassing the core *oriD* and neighbouring regions immediately upstream and downstream from the *oriD*. A tighter ternary PcrA–RepD–*oriD* complex forms in the presence of PcrA with strong contacts extending upstream from the core *oriD* but limited downstream to the end of ICR III. In the presence of nucleotides the ternary complex re-organizes into a more compact structure with boundaries contracting strictly within the core *oriD*.

We conclude that RepD forms a complex with *oriD* extending upstream and downstream of the core *oriD*. PcrA is recruited via an interaction with RepD upstream from the core *oriD*. PcrA appears to have basal weak affinity for this region even in the absence of RepD. When ATP is bound, presumably by PcrA, a conformational change reorganizes the RepD–PcrA complex strictly within the boundaries of core *oriD*.

MATERIALS AND METHODS

Protein purifications

Bacillus stearothermophilus PcrA and staphylococcal RepD used in this study were purified as described elsewhere (10). RepD mutant R189K was purified using the same method as the wild-type RepD.

Gel shift assays

A 280 bp PCR fragment containing the core *oriD* sequence was amplified using pCERoriD as template and the oligonucleotides oriD(r)NdeI (5′-TTAGCTCACTCAT ATGGCACCCCAGGCT-3′) and oriD(d)NcoI (5′-GAT GTGCTCCATGGCGATTAAGTTGG-3′), containing NdeI and NcoI restriction sites, respectively. The *oriD*-containing DNA fragment was gel purified and 5′-end-labelled in a reaction with T4 polynucleotide kinase 10 U (NEB) and 10 pmol γ-[^{32}P]-ATP (3000 Ci mmol^{-1}) (Perkin Elmer). The unincorporated γ-[^{32}P]-ATP was removed using MicroSpin™ S200 HR columns (GE Healthcare). Binding reactions were carried out with RepD, PcrA and RepD plus PcrA (concentrations are indicated in figure legends) in 15 µl binding buffer (50 mM Tris–HCl pH 7.5, 200 mM KCl), in the presence of 0.1 nM radiolabelled *oriD*-containing DNA fragment, and in the presence or absence of 0.1 µg polydIdC non-specific competitor DNA (Sigma). When indicated, 2 mM of ADP or ADPNP and 5 mM $MgCl_2$ were included. Binding reactions were incubated at 30°C for 15 min and samples were applied to a 6% non-denaturing polyacrylamide gel for electrophoresis in 1× TBE (Tris Borate EDTA) buffer. When nucleotides and $MgCl_2$ were present EDTA was omitted from the electrophoresis buffer. Gels were dried and imaged using a Molecular Imager FX and associated software (BioRad).

DNaseI footprinting

DNaseI footprinting experiments were carried out as described elsewhere (22). Purified RepD and/or PcrA proteins were incubated with 0.37 pmol supercoiled pCERoriD in 50 µl binding buffer for 1 min at 30°C. Then 50 µl of DNaseI buffer were added to the reaction (40 mM Tris–HCl pH 7.9, 10 mM NaCl, 6 mM $MgCl_2$, 1 mM $CaCl_2$) and the mixture was incubated for another 1 min at 37°C, before addition of 10 U DNaseI (Roche). Reactions were incubated at 37°C for 3 min and stopped by addition of 100 µl stop buffer (SDS 1% v/v, 200 mM NaCl, 20 mM EDTA). The digested fragments were purified by phenol:chloroform (1:1) extraction and ethanol precipitation, after addition of 20 µg/µl glycogen as DNA carrier. DNA was suspended and quantified using a Nanodrop prior to primer extension analysis. The following control reactions were included: DNA untreated with DNaseI, RepD or PcrA, DNA treated with DNaseI in the absence of RepD and/or PcrA and DNA incubated with RepD or PcrA, without DNaseI.

Primer extension analysis

The same oligonucleotides oriD(r)NdeI and oriD(d)NcoI that were used to amplify the *oriD*-containing fragment for gel shift assays were also used in primer extension reactions. They were designed to anneal to the (+) and (−) strands, respectively, outside the *oriD* region in pCERoriD. The DNaseI digested fragments were probed by primer extension using the fmol DNA cycle sequencing system from Promega, according to the manufacturer's instructions. Primer extension reactions contained

40 fmol of DNaseI digested pCERoriD, 1.2 pmol of the appropriate 5′-γ[^{32}P]-end-labelled oligonucleotide primer, 5 U of sequencing grade Taq DNA polymerase and 160 pmol of each deoxyribonucleoside triphosphate (dNTP) in 50 mM Tris–HCl pH 9.0, 10 mM $MgCl_2$. Dideoxy nucleotide sequence ladders were prepared according to the manufacturer's instructions, using 40 fmol of non-digested pCERoriD as template. Conditions for amplification were: 1× (95°C for 2 min), 30 × (95°C for 30 s; 54°C for 30 s; 70°C for 1 min). Reactions were stopped by addition of sequencing stop solution (10 mM NaOH, 95% (v/v) formamide, 0.05% (w/v) bromophenol blue, 0.05% (w/v) xylene cyanol) and then resolved through a urea-denaturing 6% polyacrylamide sequencing gel. Gels were dried and imaged using a Molecular Imager FX and associated software (BioRad).

Exonuclease III footprinting

ExoIII footprinting experiments were carried out as described elsewhere (23,24). A 280 bp 5′-end radiolabelled PCR fragment containing the *oriD* was digested with NcoI or NdeI (NEB) for 4 h at 37°C and then purified using a QIAquick PCR purification kit (QIAGEN). RepD and/or PcrA were incubated with 10 nM NcoI or NdeI digested *oriD*-containing DNA in 50 µl binding buffer for 1 min at 30°C. Then, 50 µl Exo III buffer (10 mM Bis-Tris–Propane–HCl pH 7.0, 10 mM $MgCl_2$, 1mM dithiothreitol) and 10 U Exo III (NEB) were added to the mixture. Reactions were incubated for 5, 10 or 15 min at 37°C and terminated by addition of 100 µl stop buffer. The digested DNA fragments were purified by phenol: chloroform (1:1) extraction and ethanol precipitation, after addition of 20 µg/µl glycogen. DNA was suspended in sequencing stop solution and resolved through a urea-denaturing 6% polyacrylamide sequencing gel. Gels were dried and imaged using a Molecular Imager FX and associated software (BioRad).

Analytical ultracentrifugation

The DNA substrate used in analytical ultracentrifugation (AUC) experiments was prepared by PCR using the same oligonucleotides as in the gel shift assays. Fluorescein labels were attached at the 5′-end of both oriD(r)NdeI and oriD(d)NcoI oligonucleotides to obtain the fluorescently labeled *oriD*-containing DNA fragment. AUC experiments were carried out in an Optima XL-A analytical ultracentrifuge (Beckman-Coulter, USA) retro-fitted with laser scanning fluorescence optics (Aviv Scientific, MA, USA). Binding reactions (80 µl) contained 5 nM *oriD*-DNA in 50 mM Tris–HCl pH 7.5, 200 mM KCl in the presence of 0.1 µg polydIdC and various concentrations of proteins as indicated for individual experiments. Samples were loaded into custom made 80 µl volume 3-mm path-length 2-channel sedimentation velocity cells (SpinAnalytical, NH, USA) and loaded into an AN60Ti rotor. The loaded rotor was temperature equilibrated at 30°C for 1 h prior to the run and all sedimentation velocity experiments were carried out at 35 000 r.p.m., at this temperature. Fluorescence data were obtained at an excitation wavelength of 488 nm and emission wavelengths >505 nm, scanning every cell simultaneously every 98 s. The photomultiplier settings were 100 V, at gain setting of 8. Total fluorescence signal for all cells was around 300 counts, and the signal-noise ratio for all the cells was around 30–40. Data were processed and analysed using SEDFIT (25). Molecular weights and partial specific volumes were calculated within the analysis program. Buffer densities and viscosities were determined empirically at 30°C using an Anton Paar DMA5000 density and automated viscometer, respectively. Final data were plotted as sedimentation coefficient versus RepD or PcrA concentrations and fitted to a one site binding hyperbola using GraphPad Prism.

Atomic force microscopy

Samples (30 µl) were prepared in K100 buffer (50 mM Tris–HCl pH 7.5, 1 mM EDTA, 100 mM KCl, 10 mM $MgCl_2$ and 10% (v/v) ethanediol) with 8.3 nM pCERoriD, 16.6 nM wild-type RepD or R189K and/or 16.6 nM PcrA and 1 mM ADPNP, as indicated. Samples were incubated for 20 min at 30°C to ensure complex formation. A 353 bp DNA fragment containing the core *oriD* was excised from pCERoriD by restriction with 20 units of PvuII-HF™ (New England Biolabs) for 1 h at 37°C. A sample of 10 µl from the reaction mixture was added to 40 µl of spermidine buffer (20 mM Tris–HCl, pH 7.5, 20 mM KCl, 300 µM spermidine) and 20 µl of the resulting mixture was deposited on a freshly cleaved mica surface. The sample was incubated at room temperature for 1 min followed by washing with 0.22 µm filtered, sterilized and deionized water and then dried under nitrogen gas before imaging.

Imaging was carried out in air using a Multimode Nanoscope IIIa Atomic force microscopy (AFM) (Veeco, Santa Barbara, CA, USA) in Tapping Mode™. Rectangular silicon cantilevers (Olympus, Japan) with integrated tips were used with a typical spring constant of 42 N/m and a resonant frequency around 300 kHz. The cantilevers were driven at their resonant frequency and the scan line frequency was 2 Hz at 512 × 512 pixel resolution. Typical scan sizes were 2 × 2 µm from which DNA–protein complexes were magnified using the Nanoscope software (version 5.13r3, Veeco) to generate 300 × 300 nm images. The total number of images in each case, *n*, is given in the 'Results' section. Contour lengths and bend angles were measured using the section analysis and angle tools, respectively, of the same software.

RESULTS

ExoIII probing at the front of *oriD*

The 5′-end of the (−) strand of the *oriD* containing DNA fragment was radioactively labelled and ExoIII digestion was carried out in the presence and absence of RepD and PcrA, as shown in Figure 1. In the absence of proteins, ExoIII was able to digest the (−) strand through the *oriD* (see control lane 3 in Figure 1A–D), whereas in the presence of RepD an initial protection point from

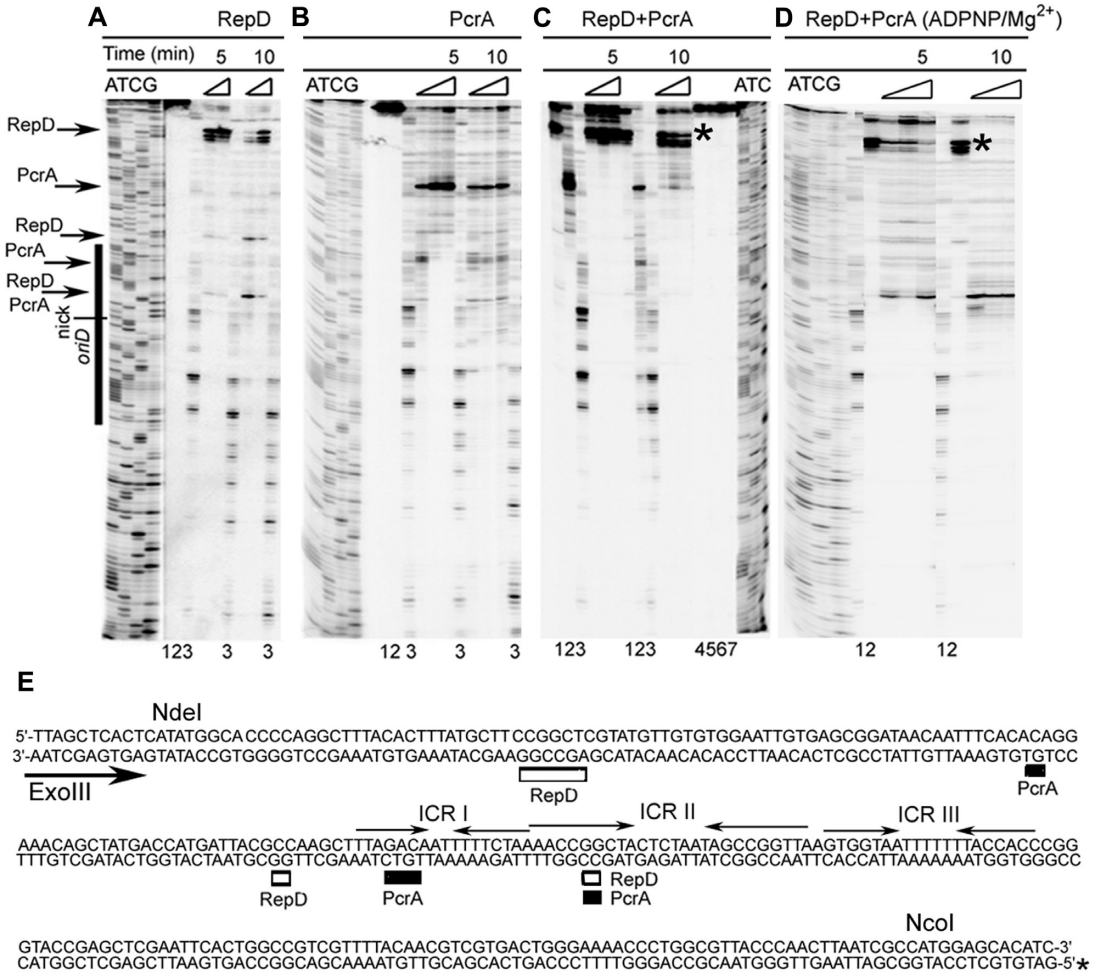

Figure 1. ExoIII footprinting of the *oriD* (−) strand. ExoIII footprinting was carried out in the presence of RepD (**A**), PcrA (**B**), RepD+PcrA (**C**) and RepD+PcrA+ADPNP/Mg^{2+} (**D**). The complete sequence of *oriD* containing DNA used in these experiments is shown in (**E**) with the ICR I, ICR II and ICR III sites marked by converging arrows. The asterisk at the 5′-end of the (−) strand (bottom strand) indicates the radioactive phosphate. The 3′–5′ direction of the ExoIII digestion is indicated by an arrow starting at the 3′-end of the (−) strand. For clarity, the ExoIII resistance points have been marked by white (RepD) and black (PcrA) boxes along the sequence of the probe and by labelled arrows next to the sequence ladder. The precise position of *oriD* in the sequence ladder is indicated by a vertical black bar and the position where RepD nicks the DNA within *oriD* is also indicated. The gel in (A) shows ExoIII digestions of the radioactively labelled probe for 5 and 10 min in the presence of 0.1 and 0.2 μM RepD. Only the lanes with controls are numbered at the bottom of the gel representing undigested probe in the absence of proteins (lane 1), undigested probe incubated with 0.2 μM RepD (lane 2) and probe in the absence of proteins digested with ExoIII for 5 and 10 min (lanes 3). The gel in (B) shows ExoIII digestions of probe for 5 and 10 min in the presence of 0.2, 0.5 and 1.0 μM PcrA. Only the lanes with controls are numbered at the bottom of the gel representing undigested probe in the absence of proteins (lane 1), undigested probe incubated with 1.0 μM PcrA (lane 2) and probe in the absence of proteins digested with ExoIII for 5 and 10 min (lanes 3). The gel in (C) shows ExoIII digestions of probe for 5 and 10 min in the presence of constant 0.2 μM RepD with 0.2, 0.5 and 1.0 μM PcrA. Only lanes with controls are numbered at the bottom of the gel representing probe incubated with 0.2 μM RepD and digested with ExoIII for 5 and 10 min (lanes 1), probe incubated with 1.0 μM PcrA and digested with ExoIII for 5 and 10 min (lanes 2), probe digested with ExoIII in the absence of proteins for 5 and 10 min (lane 3), undigested probe in the absence of proteins (lane 4), undigested probe incubated with 0.2 μM RepD (lane 5), undigested probe incubated with 1.0 μM PcrA (lane 6) and undigested probe incubated with 0.2 μM RepD and 1.0 μM PcrA (lane 7). The point of strong resistance to ExoIII digestion is marked by an asterisk. The gel in (D) shows ExoIII digestions of probe for 5 and 10 min in the presence of constant 0.2 μM RepD, 50 μM ADPNP, 200 μM $MgCl_2$, with 0.2, 0.5 and 1.0 μM PcrA. Only lanes with controls are numbered at the bottom of the gel representing probe digested with ExoIII in the absence of proteins for 5 and 10 min (lanes 1) and probe incubated with 0.2 μM RepD and 1.0 μM PcrA digested with ExoIII for 5 and 10 min (lanes 2). The asterisk indicates the strong resistance to ExoIII digestion in the presence of RepD and PcrA.

ExoIII digestion was located ~74–80 bp upstream from the ICR I site (Figure 1A). Further resistance points were detected just in front of the ICR I site and in the first half of the ICR II site.

In the presence of RepD and PcrA, the first resistance point ~74–80 bp upstream from the ICR I site, became considerably stronger as the ExoIII was unable to pass this point even after 10 min digestion (Figure 1C).

Interestingly, in the presence of only PcrA three resistance points were evident on the (−) strand as the ExoIII approached the ICR I site. One strong resistance point at ~35 bp upstream from the ICR I site, and two weak resistance points within the first halves of the ICR I and ICR II

sites (Figure 1B). These data indicate that even in the absence of RepD, PcrA appears to bind to this DNA fragment, targeting the area upstream from the ICR I site (see gel shift data later on).

In the presence of ADPNP, a non-hydrolysable analogue of ATP, the ExoIII footprint of the ternary complex on the (−) strand changed drastically. As the ExoIII approached the ICR I site, the strong resistance at ~74–80 bp upstream from ICR I and the second resistance just in front of ICR I disappeared, whereas the resistance point within the first half of ICR II strengthened with ExoIII being unable to pass this point even after 10 min digestion (compare the ExoIII digestion patterns of RepD + PcrA in the absence and presence of ADPNP in Figure 1C and D, respectively).

ExoIII probing at the back of *oriD*

In this series of experiments, the 5′-end of the (+) strand was radioactively labelled and the DNA digested with ExoIII in the presence and absence of RepD (Figure 2A) and PcrA (Figure 2B). In the absence of proteins, ExoIII was able to digest through the ICR III and ICR II sites but then encountered strong resistance in a stretch of thymines in the middle of ICR I (see lane 3 in Figure 2A, B and lane 1 in Figure 2C and D). This was

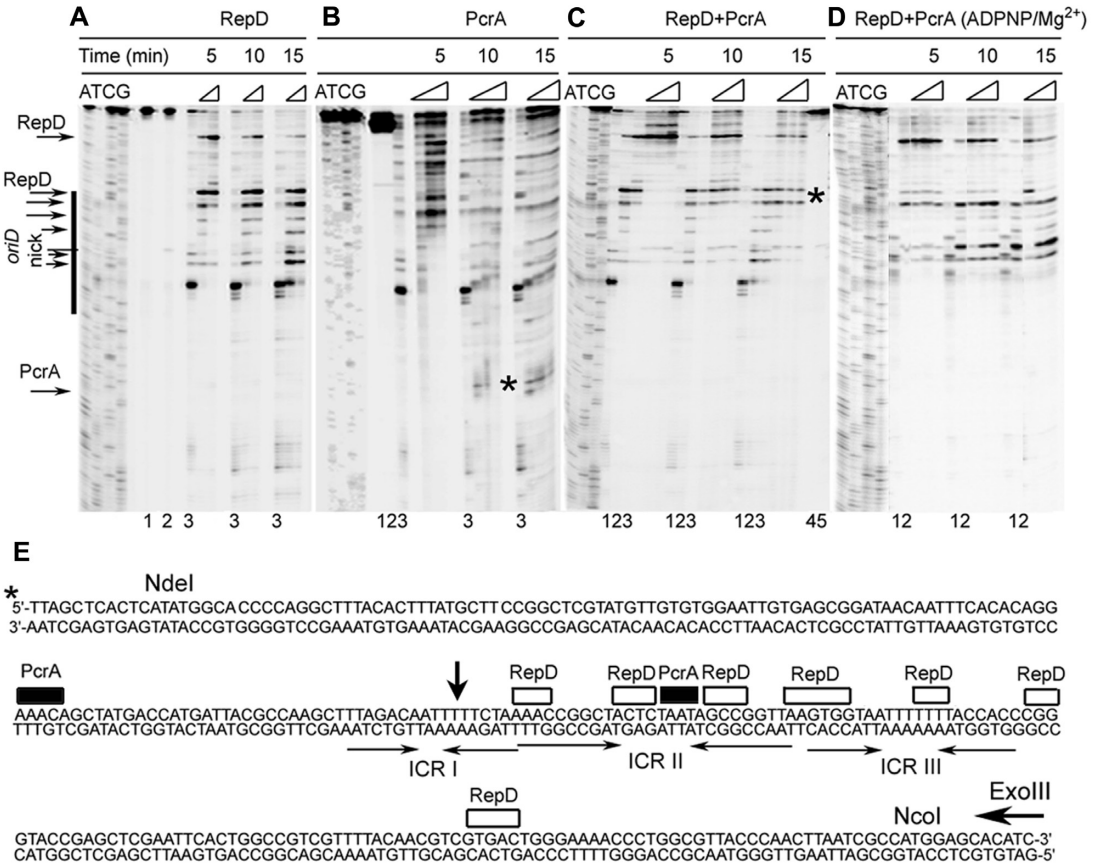

Figure 2. ExoIII footprinting of the *oriD* (+) strand. ExoIII footprinting was carried out in the presence of RepD (**A**), PcrA (**B**), RepD+PcrA (**C**) and RepD+PcrA+ADPNP/Mg^{2+} (**D**). The complete sequence of *oriD* containing DNA used in these experiments is shown in (**E**) with the ICR I, ICR II and ICR III sites marked by converging arrows. The asterisk at the 5′-end of the (+) strand (top strand) indicates the radioactive phosphate and the 3′–5′ direction of the ExoIII digestion is indicated by an arrow starting at the 3′-end of the (+) strand. For clarity the ExoIII resistance points with RepD have been marked by white boxes, and with PcrA with black boxes along the sequence of the probe and by labelled arrows next to the sequence ladder. The resistance point detected in the absence of any proteins is shown in the middle of ICR I by a vertical arrow. The precise position of *oriD* in the sequence ladder is indicated by a vertical black bar and the position where RepD nicks the DNA within the *oriD* is also indicated. The gel in (A) shows ExoIII digestions of the radioactively labelled probe for 5, 10 and 15 min in the presence of 0.1 and 0.2 μM RepD. Controls represent undigested probe in the absence of proteins (lane 1), undigested probe incubated with 0.2 μM RepD (lane 2) and probe in the absence of proteins digested with ExoIII for 5, 10 and 15 min (lanes 3). The gel in (B) shows ExoIII digestions of probe for 5, 10 and 15 min in the presence of 0.2, 0.5 and 1.0 μM PcrA. Controls represent undigested probe in the absence of proteins (lane 1), undigested probe incubated with 1.0 μM PcrA (lane 2) and probe in the absence of proteins digested with ExoIII for 5, 10 and 15 min (lanes 3). The ExoIII resistance point that coincides with the resistance point detected at the front of *oriD* in the equivalent experiment in Figure 1B is marked by an asterisk. The gel in (C) shows ExoIII digestions of probe for 5, 10 and 15 min in the presence of constant 0.2 μM RepD with 0.2, 0.5 and 1.0 μM PcrA. Controls represent probe digested with ExoIII for 5, 10 and 15 min in the absence of proteins (lanes 1), probe incubated with 0.1 μM RepD and digested with ExoIII for 5, 10 and 15 min (lanes 2), probe incubated with 0.2 μM RepD and digested with ExoIII for 5, 10 and 15 min (lanes 3), undigested probe incubated with 0.2 μM RepD (lane 4), and undigested probe incubated with 1.0 μM PcrA (lane 5). The strong ExoIII resistance point at the end of ICR III is marked by an asterisk. The gel in (D) shows ExoIII digestions of probe for 5, 10 and 15 min in the presence of constant 0.2 μM RepD, 50 μM ADPNP, 200 μM $MgCl_2$, with 0.2, 0.5 and 1.0 μM PcrA. Controls represent probe digested with ExoIII in the absence of proteins for 5, 10 and 15 min (lanes 1) and probe incubated with 0.2 μM RepD digested with ExoIII for 5, 10 and 15 min (lanes 2).

specific for the (+) strand as it was not observed on the (−) strand when the ExoIII approached from the front of the ICR I site (see control lane 3 in Figure 1A–C and lane 1 in Figure 1D). The possibility of a secondary DNA structure inhibiting ExoIII was investigated by creating mutant *oriD* fragments with mutations in ICR I (*oriDI*), ICR II (*oriDII*) and ICR III (*oriDIII*), but all mutant *oriD* fragments exhibited the same resistance point upon ExoIII digestion, albeit slightly weaker in the *oriDI* case (Supplementary Figure 1s). This resistance appears to be specific to *oriD* as a non-specific DNA fragment amplified from the empty pCER19 vector with the same oligonucleotides used to amplify *oriD* did not exhibit resistance to ExoIII digestion (Supplementary Figure 1s).

In the presence of RepD, protection from ExoIII was extended ~46–50 bp downstream from the ICR III site (Figure 2A). At longer digestions ExoIII was able to pass this point but then encountered several more resistance points starting at the end of ICR III and extending all through the ICR II and ICR I sites (compare the 5, 10 and 15 min digestions in the presence of RepD alone in Figure 2A). With PcrA alone ExoIII digested through the *oriD* containing DNA fragment but a strong resistance point was detected about 30–35 nucleotides past the ICR I site (Figure 2B the band marked by an asterisk) which coincides with the same strong resistance point detected in the equivalent experiment in Figure 1B. A second minor resistance point was apparent in the middle of ICR II.

In the presence of RepD and PcrA, the first resistance point ~46–50 bp downstream from the ICR III site on the (+) strand, remained the same as in the absence of PcrA. However, the resistance points at the end of ICR III became considerably stronger in the presence of PcrA. Even after 15 min digestion, the ExoIII was halted at the end of ICR III and could not progress into the ICR II and ICR I sites (Figure 2C; point marked by an asterisk).

We have already seen ADPNP-induced changes when we probed the (−) strand with ExoIII (see above). Similar changes were also apparent at the other end of the *oriD* on the (+) strand as the ExoIII approached the ICR III site (Figure 2D). In the presence of ADPNP, the first resistance point ~46–50 bp downstream from the ICR III site on the (+) strand became weaker (compare the gels in Figure 2C and D), the resistance points at the end of ICR III also became weaker and the ExoIII was able to progress beyond ICR III into the ICR II site (compare the ExoIII digestion patterns of RepD+PcrA in the presence and absence of ADPNP in Figure 2C and D).

DNaseI probing of *oriD*

DNaseI footprinting was carried out with the supercoiled *oriD*-containing pCERoriD in the presence and absence of RepD and PcrA. This technique ensures that any supercoiling-dependent features of the system are preserved. Both (+) and (−) strands can be probed separately using the appropriate complementary radiolabelled oligonucleotide. DNaseI footprinting analysis of the (−) strand revealed a clear footprint in the presence of RepD encompassing the core *oriD* that includes the ICR I–III sites (Figure 3A). This footprint did not change in the presence of PcrA (Figure 3B).

By comparison, DNaseI footprinting of the (+) strand revealed a clear footprint for RepD in *oriD* and an additional hypersensitive site at ~55–61 bp upstream from ICR I (Figure 4A–D). In the presence of PcrA, the footprint in *oriD* remained the same but the hypersensitive site upstream from ICR I disappeared and two other hypersensitive sites in the region extending further upstream ~62–90 bp from ICR I appeared (Figure 4E and F). The presence of ADPNP did not change the footprinting pattern of the ternary complex (Figure 4C and D).

Similar results were obtained with the mutant R189K version of RepD that nicks and attaches itself on the 5′-end of the nick but fails to religate the nick (unpublished data). ExoIII and DNaseI footprints of the (+) and (−) strands were identical to those obtained with native RepD (data not shown). An example of DNaseI footprints obtained with R189K on the (+) strand is shown in Figure 4C.

ATP-binding affects the PcrA–RepD–*oriD* ternary complex

Our ExoIII experiments described above revealed that ADPNP binding presumably by PcrA, since RepD is not known to bind ATP, somewhat affects the ternary complex (Figures 1 and 2), although this effect was not detected by DNaseI footprinting (Figure 4). In order to first verify the formation of a ternary PcrA–RepD–*oriD* complex and then the effects of ADPNP binding on the complex, we carried out gel shift assays using the same *oriD*-containing fragment that was used in ExoIII experiments described above.

First, we established that RepD binds to this DNA even in the presence of competitor polydIdC, as at increasing concentrations an initial shift followed by a second supershift at high RepD concentrations were observed (Figure 5A; gel on the left). Then we established the formation of a ternary PcrA–RepD–*oriD* complex by keeping the RepD concentration constant at 0.5 μM (a concentration at which all of the DNA substrate was shifted by RepD) and introducing increasing concentrations of PcrA. A distinct supershift was detected as the PcrA concentration increased indicating the formation of the ternary complex (Figure 5A; gel on the right). Addition of ADPNP or ADP nucleotides in the binding mixture reduced ternary complex formation (Figure 5B).

PcrA has weak affinity for *oriD*

During ExoIII probing in the presence of PcrA we detected two resistance sites at the front of *oriD*. A stronger site at ~35 bp upstream from the ICR I site (within the pCER19 vector sequence) and a weaker site within the first half of the ICR I site (Figure 1B). Therefore, even in the absence of RepD, PcrA appears to bind upstream of *oriD*. PcrA is not known to have affinity for any specific dsDNA sequence. It does, however, bind dsDNA apparently with weak affinity, since binding was detected using a classical gel shift

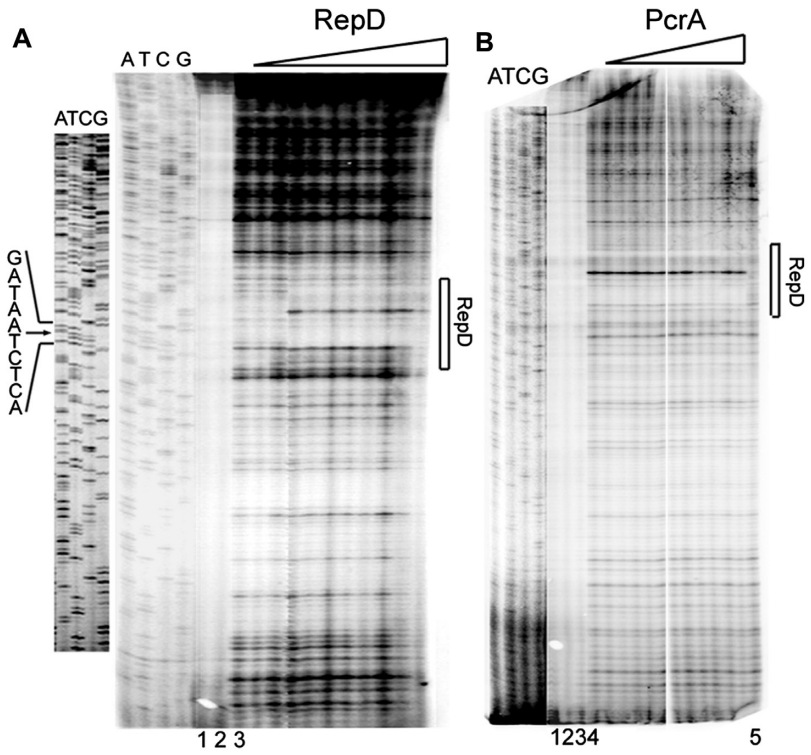

Figure 3. DNaseI footprinting of the (−) strand. The gel in (**A**) shows DNaseI footprinting in the presence of RepD only. The DNA sequence of the complementary (+) strand is shown and the position of the nick within the *oriD* is indicated by an arrow. Primer extension reactions were carried out with radioactively labelled oriD(r)NdeI oligonucleotide using plasmid pCERoriD incubated with increasing concentrations of RepD (5, 10, 50, 80, 100, 150, 200, 500, 1000 and 2000 nM) and digested with DNaseI. Controls represent primer extension reactions with undigested pCERoriD in the absence of RepD (lane 1), undigested pCERoriD in the presence of 500 nM RepD (lane 2) and digested pCERoriD in the absence of RepD (lane 3). The RepD footprint is indicated by a bar for clarity. The gel in (**B**) shows DNAaseI footprinting in the presence of RepD and PcrA. The DNA sequence of the complementary (+) strand is shown for clarity. Primer extension reactions were carried out with radioactively labelled oriD(r)NdeI oligonucleotide using plasmid pCERoriD incubated with 80 nM RepD and increasing concentrations of PcrA (10, 50, 80, 100, 150, 200, 500, 1000, 2000, 4000 and 8000 nM). Controls represent primer extension reactions with undigested pCERoriD (lane 1), undigested pCERoriD in the presence of 80 nM RepD (lane 2), undigested pCERoriD in the presence of 80 nM RepD and 8000 nM PcrA (lane 3), digested pCERoriD in the presence of 80 nM RepD (lane 4) and digested pCERoriD in the absence of proteins (lane 5).

assay only in the absence of competitor DNA (Figure 5C). There is no higher affinity for *oriD* because shifts observed with *oriD*-containing and a non-specific fragments were comparable (data not shown).

The stoichiometry of the RepD–*oriD* complex

The formation of the initiation complex was studied by velocity sedimentation AUC experiments to obtain information of the stoichiometry of the RepD–*oriD* and PcrA–RepD–*oriD* complexes (Figure 6). Incubation of 5 nM of the same *oriD*-containing DNA fragment (fluorescein labelled at the 5′-ends of both strands) as the one used in our gel shift assays with increasing concentrations of RepD resulted in the formation of complexes with increasing sedimentation coefficients (Figure 6A). A plot of the sedimentation coefficients versus [RepD] produced a biphasic curve, with a steep increase in the first phase up to a RepD concentration of ~60–80 nM and a shallow increase in the second phase up to a RepD concentration of 7.375 μM (Figure 6A). We interpret these data as follows. The first phase shows the formation of the specific *oriD*–RepD complex and the second phase shows the formation of a non-specific *oriD*–RepD complex consistent with our gel shift assays shown in Figure 5A. Considering *oriD* as a single RepD-binding site and fitting the first phase (0–1.25 μM RepD) to a single site binding hyperbola, using GraphPad Prism, produced a good fit ($R^2 = 0.961$) with an apparent K_d of 124 nM and a stoichiometry of approximately 1 DNA: 10 RepD (Figure 6A). This apparent stoichiometry should be considered with caution as binding of RepD to *oriD* appears to be rather weak and thus a mixture of free and complexed DNA would be present both of which have different buoyancy. Present methods are unable to distinguish between such species. Another complication is that there are potentially three RepD-binding sites (ICR I–III) within *oriD* with potential cooperativity at play that complicate theoretical binding models. Complications also arise from the effect of shape changes. Free DNA would be quite flexible in solution adopting a number of conformations. As RepD binds the DNA would become more rigid and any additional RepD-induced changes such as bending (see below) would complicate buoyancy comparisons.

To investigate binding of PcrA to the *oriD*–RepD complex, we incubated 5 nM *oriD*–DNA with 600 nM

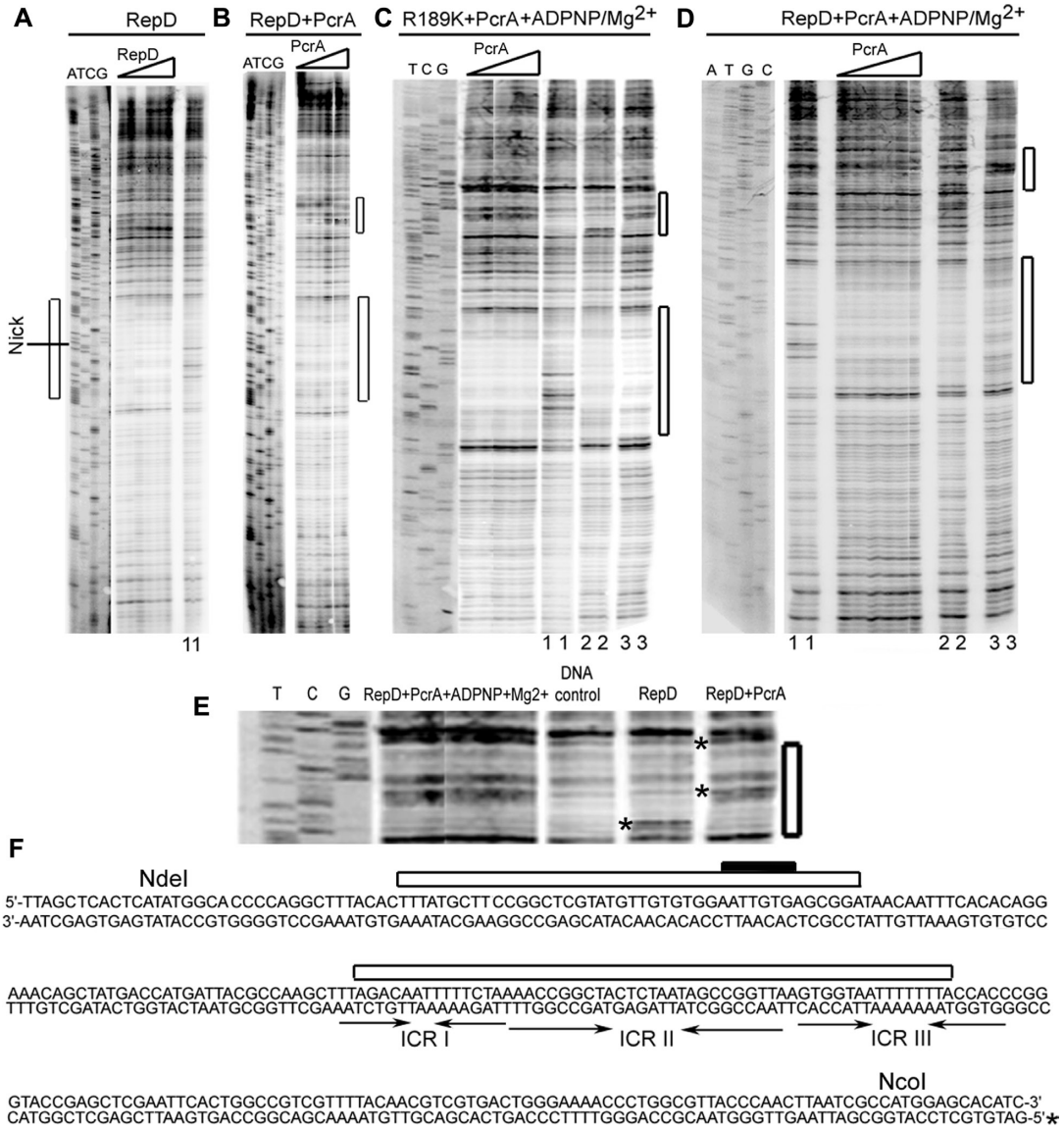

Figure 4. DNaseI footprinting of the (+) strand (nicked strand). (**A**) DNAaseI footprinting in the presence of increasing amounts of RepD only. The DNA sequence of the complementary (−) strand is shown and the position of the nick within the *oriD* is indicated. Primer extension reactions were carried out with radioactively labelled oriD(d)NcoI oligonucleotide using plasmid pCERoriD incubated with increasing concentrations of RepD (50, 100, 150, 200, 500 and 1000 nM) and digested with DNaseI. Controls in lanes 1 represent primer extension reactions with digested pCERoriD in the absence of RepD. (**B**) Primer extension reactions from pCERoriD digested in the presence of 800 nM RepD and increasing concentrations of PcrA (50, 100, 200, 500, 1000, 2000 nM). (**C**) Primer extension reactions carried out in the presence of 100 nM R189K, 50 μM ADPNP, 200 μM $MgCl_2$ and increasing concentrations of PcrA (50, 100, 200, 500, 1000 and 2000 nM). Controls in lane 1 represent primer extension reactions from pCERoriD digested in the absence of any proteins, in lane 2 reactions from pCERoriD digested in the presence of 100 nM R189K in the absence of ADPNP and $MgCl_2$, in lane 3 reactions from pCERoriD digested in the presence of 100 nM R189K, 500 nM PcrA in the absence of ADPNP and $MgCl_2$. (**D**) Primer extension reactions carried out using pCERoriD digested in the presence of 100 nM RepD, 50 μM ADPNP, 200 μM $MgCl_2$ and increasing concentrations of PcrA (50, 100, 200, 500, 1000 and 2000 nM). Controls in lane 1 represent primer extension reactions from pCERoriD digested in the absence of any protein, in lane 2 reactions from pCERoriD digested in the presence of 100 nM RepD in the absence of ADPNP and $MgCl_2$, in lane 3 reactions from pCERoriD digested in the presence of 100 nM RepD, 500 nM PcrA in the absence of ADPNP and $MgCl_2$. (**E**) Magnification of the footprint detected in the presence of PcrA, with or without ADPNP, from the R189K + PcrA experiments is shown and the differences between minus and plus PcrA are marked by asterisks for clarity. (**F**) The complete sequence of the *oriD* containing probe used in these experiments is shown at the bottom of the figure with the ICR I, ICR II and ICR III sites marked by converging arrows. The precise positions of the DNaseI footprints in the sequence are indicated by horizontal white bars. The same footprints are also indicated by vertical white bars next to the gels for clarity. The black bar indicates the precise position of the DNaseI hypersensitive site observed in the presence of RepD. The position where RepD nicks the DNA within the *oriD* is indicated in the sequence of the far left gel.

RepD to allow the formation of the *oriD*–RepD complex and then added increasing concentrations of PcrA (Figure 6B). The excess of RepD was used to ensure that all of the *oriD*–DNA was sequestered at all times in the RepD–*oriD* complex. A plot of sedimentation coefficients versus PcrA concentration produced a curve with two phases. An initial increase followed by a plateau up to 2 μM PcrA followed by a further increase up to 8.25 μM

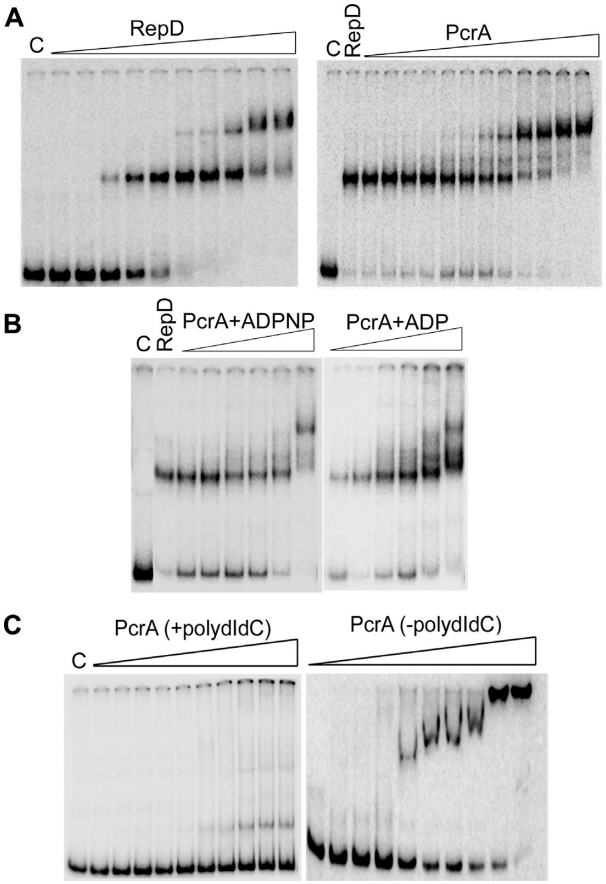

Figure 5. The effects of nucleotides on the *oriD*–RepD–PcrA complex. (**A**) Detection of the ternary *oriD*–RepD–PcrA complex by gel shift assays. The gel on the left shows binding of RepD (0.01, 0.05, 0.08, 0.1, 0.2, 0.5, 1, 2, 4 and 5 μM) to a radioactively labelled linear DNA fragment (0.1 nM) containing the *oriD*. Binding reactions were carried out in 50 mM Tris–HCl pH 7.5, 200 mM KCl, 0.1 μg/μl polydIdC at 30°C for 15 min. Control C shows the radioactive probe in the absence of RepD. The gel on the right shows binding of PcrA (0.01, 0.05, 0.08, 0.1, 0.2, 0.5, 1, 2, 4, 5, 8 and 10 μM) in the presence of 0.5 μM RepD. Experimental conditions were as described in (A). Control C shows the radioactive probe in the absence of proteins and the lane next to C shows binding of RepD (0.5 μM) in the absence of PcrA. (**B**) The effect of ADPNP and ADP on *oriD*–RepD–PcrA ternary complex. The gel shows binding of PcrA (0.05, 0.1, 0.5, 1, 5 and 10 μM) in the presence of 0.5 μM RepD, 2 mM nucleotides (ADP and ADPNP) and 5 mM $MgCl_2$. Control C shows the radioactive probe in the absence of proteins and the lane next to C shows binding of RepD (0.5 μM) in the absence of PcrA. (**C**) Gel shift assays using 0.1 nM of the 280 bp *oriD* containing probe with increasing concentrations of PcrA (0.01, 0.05, 0.08, 0.1, 0.2, 0.5, 1, 2, 4 and 5 μM) in the presence (left gel) of 0.1 μg/μl of polydIdC and PcrA (0.01, 0.05, 0.1, 0.2, 0.4, 0.6, 0.8, 1, 2 and 5 μM) in the absence of polydIdC (right gel). Binding reactions were carried out in 50 mM Tris–HCl pH 7.5, 200 mM KCl at 30°C for 15 min. Lane C shows the probe in the absence of PcrA.

PcrA (Figure 6B). In a control experiment, without RepD in the binding reaction the initial phase up to 2 μM PcrA was absent and only the second phase from 1 to 8.25 μM PcrA was apparent (Figure 6C). These data are consistent with an initial specific recruitment of PcrA by RepD manifested in the first phase up to 2 μM PcrA. The increase of the sedimentation coefficient observed at higher PcrA concentrations is presumably due to non-specific interactions of PcrA with the *oriD*-PcrA complex. The combined AUC data are entirely consistent with our gel shift data shown in Figure 5. Fitting of the first phase to a single site binding hyperbola produced a fit with $R^2 = 0.903$ and an apparent K_d of 98.5 nM for binding of PcrA to the *oriD*–RepD complex. The apparent stoichiometry of PcrA relative to RepD is 1:10 but deconvoluting the precise stoichiometry of the ternary complex with this method is not possible for reasons explained above.

RepD bends *oriD*

A 353 bp DNA fragment containing *oriD* was imaged by AFM in the presence of RepD or R189K with PcrA and ADPNP, as appropriate (Figure 7). To ensure preservation of supercoiling effects and efficient covalent linkage of RepD or R189K to *oriD* we first assembled all complexes on supercoiled pCERoriD, then excised an *oriD*-containing 353 bp DNA fragment by PvuII digestion before imaging. In the absence of proteins, typical images were observed with no high or globular features ($n = 50$) (Figure 7A, a1–a4). There was considerable flexibility in the molecules observed and many displayed an asymmetrically located bend (such as Figure 7A, a3). In the 353 bp fragment used, *oriD* is also located asymmetrically, the nick site at the centre of the *oriD* sequence being 213 bp from the 5′-end of the molecule. Although the orientation of the DNA fibre is unknown, in one of two scenarios this observation is in agreement with electrophoretic mobility shift experiments which demonstrated the presence of an intrinsic bend in the closely related *oriC* sequence in the absence of any protein (26). For the 50 naked DNA molecules imaged by AFM, the average contour length was 109.8 ± 8.9 nm, slightly shorter than 115.4 nm predicted for B-form DNA with 10.4 base pairs per turn and a pitch of 3.4 nm. Yields of the 353 bp fragment on the mica surface in the absence of any protein were low because the spermidine buffer used favored the binding of DNA-protein complexes.

In the presence of RepD, a high, globular feature was seen on the DNA, which was localized at the bend in the DNA fibre (Figure 7A, b1–b4). This was also seen for the active site mutant R189K, which does not religate the nicked *oriD* sequence, forming a more stable covalent DNA-protein complex than the wild-type RepD. From 100 images of each complex the contour lengths of the DNA arms extending from the globular feature were measured (Supplementary Table 1). The average total length of DNA for all complexes was marginally shorter than for free DNA (108.0 ± 9.4 nm for RepD, 101.1 ± 9.9 nm for R189K), although some variation in individual length was noted. From the relative lengths of the DNA arms extending from the globular feature, the latter is placed at 65% along the length of the fragment. This corresponds to the 5′ side of ICR III (27) and therefore in agreement with previous work on binding of RepD with *oriD* as well as studies of RepC bound to *oriC* (26).

The angle between the DNA arms at the globular feature was measured for each image. Histograms depicting the bend angles (Figure 8) suggest two principal types of complex, one characterized by a bend angle of

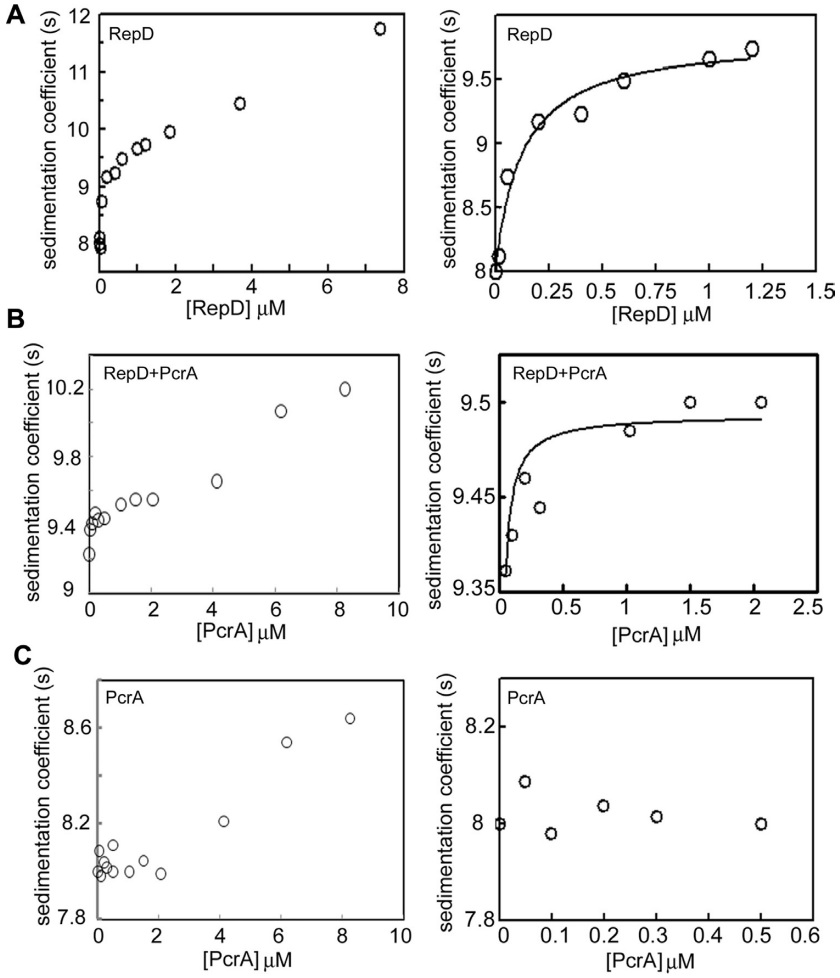

Figure 6. Sedimentation analysis of the initiation complexes. (**A**) Fluorescein labelled *oriD*-DNA (5 nM) was incubated with increasing concentrations of RepD (0, 0.02, 0.04, 0.06, 0.2, 0.4, 0.6, 1, 1.2, 1.844, 3.688 and 7.375 μM) and the complexes were subjected to sedimentation AUC analysis as described in 'Materials and Methods' section. Plots of the sedimentation coefficient(s) versus RepD concentration are shown for the entire RepD titration (left graph) and the first phase 0–1.2 μM RepD (right graph). The latter was fitted to a one site binding hyperbola. (**B**) The DNA substrate was incubated initially with 600 nM RepD and then increasing concentrations of PcrA were added (0, 0.05, 0.1, 0.2, 0.3, 0.5, 1.03, 1.5, 2.062, 4.125, 6.187 and 8.25 μM). Plots of the sedimentation coefficient(s) versus PcrA concentration are shown for the entire PcrA titration (left graph) and the initial range 0–2.062 μM PcrA (right graph). (**C**) The same experiment as in panel B was carried out in the absence of RepD. Plots of the sedimentation coefficient(s) versus PcrA concentration are shown for the entire PcrA titration (left graph) and the first phase 0–0.5 μM PcrA (right graph). The latter was fitted to a one site binding hyperbola.

around 90° and another with a broader distribution about 140–150°. Complexes were thus classified into one of two types depending on whether the bend was acute or obtuse. The two types were named 'sharp' and 'shallow' if the bend was less or greater than 110° relative to the axis of the DNA backbone, respectively. The sharp-angled complexes comprised 39% and 35% of the imaged populations for complexes containing RepD and R189K, respectively. These populations also had a slightly smaller contour length than their shallow-angled counterparts (Supplementary Table S1).

RepD-mediated recruitment of PcrA induces additional *oriD* bending

In the presence of PcrA with RepD or R189K (Figure 7A, c1–c4), the proportion of sharply bent DNA fragments observed increased to 60% and 57%, respectively, for 100 images of each complex. The distribution of bend angles (Figure 8) was also seen to focus about the principal angles for each complex upon the addition of PcrA, suggesting that complexes of intermediate angle were more likely to be resolved to the sharp-angled classification in the RepD:PcrA complex. As before, the average contour length of each sharply-angled population was slightly smaller than that of the shallow-angled molecules.

When ADPNP was included with RepD and PcrA or R189K and PcrA (Figure 7A, d1–d4) the number of sharply bent DNA fragments decreased to 41% and 46%, respectively, again for 100 images of each complex. The histograms (Figure 8) show that the focus about each principal angle is reduced once more, with an increase in the number of

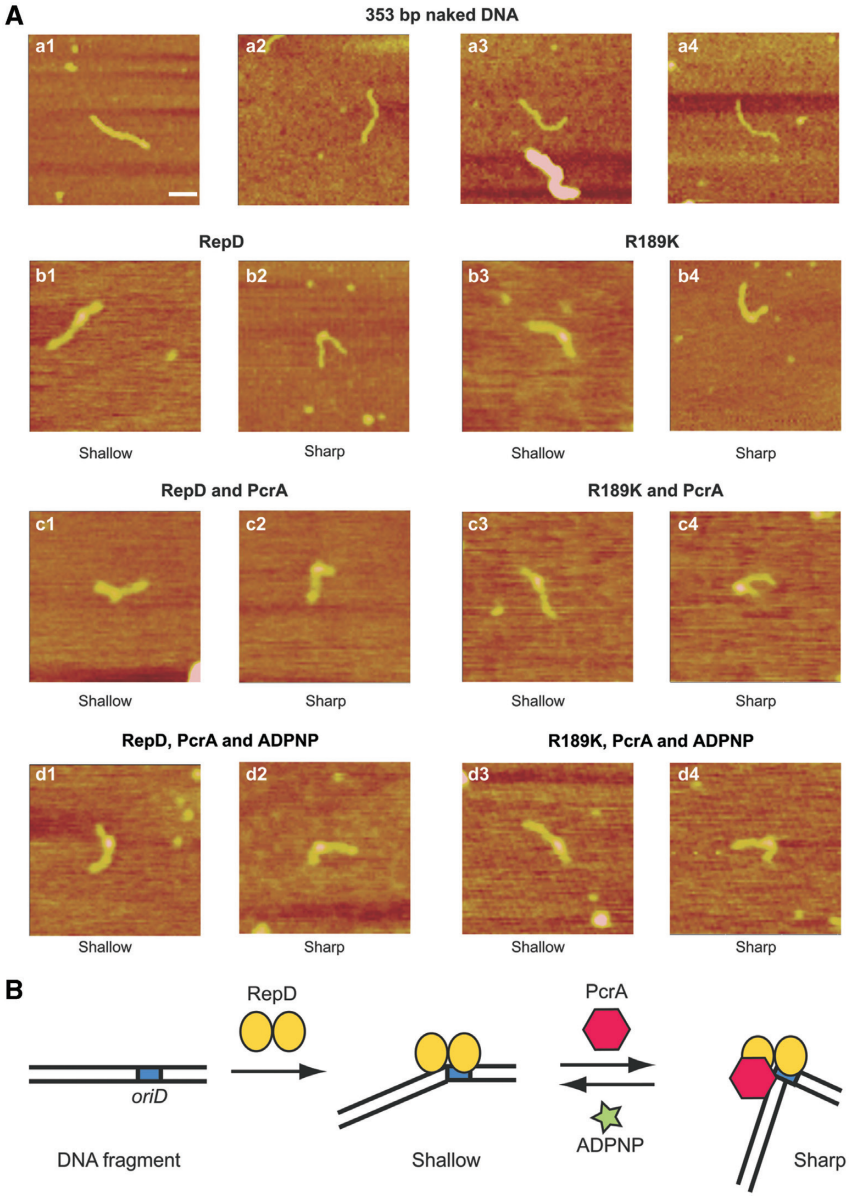

Figure 7. AFM images of complexes. (**A**) Tapping mode AFM images in air of the 353 bp DNA fragment containing the core *oriD* deposited on mica (a1–a4). Where indicated, RepD, R189K, PcrA and ADPNP are also present (b1–b4, c1–c4, d1–d4). The resultant DNA–protein complexes are divided into two categories depending on the angle induced by the bound protein: sharp and shallow. Representative software zoomed images at 300 × 300 nm are shown. The number of complexes observed and measured is given in the text. Scale bar is 50 nm. (**B**) Schematic interpretation of AFM data (not to scale) for RepD or R189K binding to *oriD* and subsequent recruitment of PcrA and ADPNP. The location of *oriD* is asymmetric in the 353 bp DNA fragment; the population of molecules exhibiting sharp angles is favoured upon addition of PcrA, although subsequent remodelling upon addition of ADPNP favours the shallow angles.

intermediate-angled molecules suggesting that the remodelled protein–DNA complex is more flexible. Summarizing the AFM data (Figure 7B), we conclude that the naked DNA is able to adopt a variety of conformations, including the presence of an asymmetric bend within *oriD*. Binding of Rep results in a bend at a defined position along the length of the DNA which is consistent with the location of *oriD* within the DNA fragment, and recruitment of PcrA biases the population towards one with a sharper bend angle. However, when PcrA binds ADPNP this population is once again reduced.

DISCUSSION

RepD forms an extended loose complex with *oriD*

Mapping the boundaries of the RepD–*oriD* complex by ExoIII footprinting revealed that protection from ExoIII in the presence of RepD was extended ~74–80 bp upstream from the ICR I site and 46–50 bp downstream from the ICR III site. The downstream protection site was somewhat weaker than the upstream site, as it was reduced more readily by ExoIII digestion for 15 min. In both cases, as the ExoIII approached the *oriD* on the (−) strand from the ICR I site or the (+) strand from

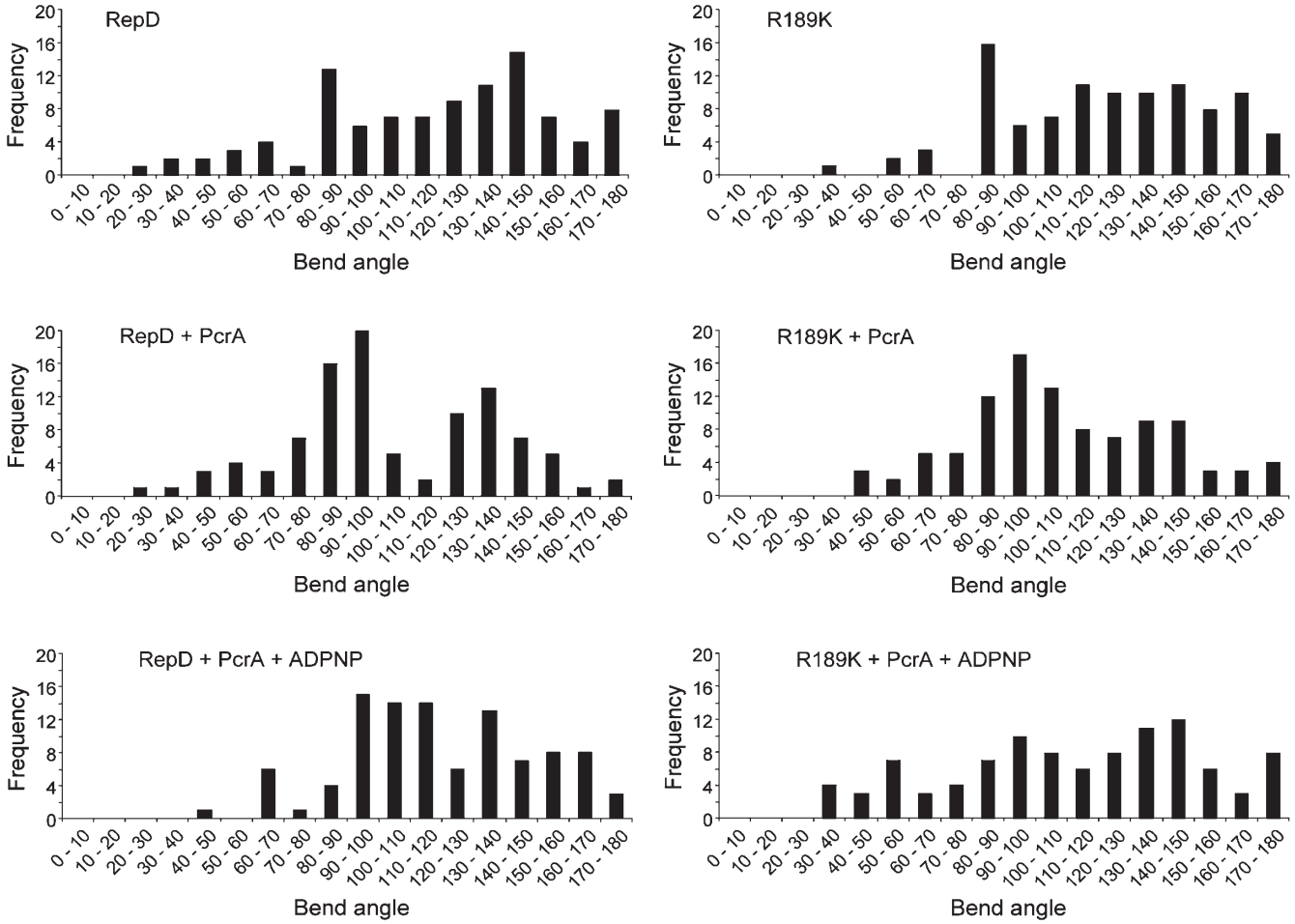

Figure 8. Distribution of bend angles. The angle between the DNA arms at the globular feature of each AFM image was measured for 100 images of each combination of Rep protein, PcrA and ADPNP as indicated. Molecules were classified into bend angle ranges and counted; the frequency of each bend angle range is shown.

the ICR III site, there were strong protection points at the beginning of ICR I and end of ICR III, respectively, indicating strong interactions of bound RepD molecules with the core *oriD* sequence. After digestion of the (−) strand for 15 min the ExoIII managed to pass the resistance point at the beginning of ICR I but then halted at a second strong resistance point within the first half of the ICR II site. By comparison, on the (+) strand after 15 min digestion as the ExoIII approached from the ICR III site it encountered several additional resistance points beyond the ICR III end boundary and within the ICR I, ICR II and ICR III sites. By comparison, DNaseI footprinting did not reveal protection outside the core *oriD* boundaries but did reveal an additional hypersensitive site 55–61 bp upstream from ICR I. This is probably because in the extended RepD–DNA complex the DNA outside the core *oriD* is still accessible to DNaseI. These data are consistent with an extended, loose RepD–*oriD* complex with strong interactions of RepD within the core *oriD* including the ICR I–III sites and additional weak interactions extending upstream and downstream beyond *oriD*. An *oriD*–RepD complex of five RepD dimers bound to *oriD* based upon the apparent stoichiometry from the AUC data is shown in the model of Figure 9.

PcrA is recruited upstream from the ICR I site

In the presence of RepD and PcrA, the resistance point 74–80 bp upstream from the ICR I site on the (−) strand became considerably stronger, whereas the resistance point 46–50 bp downstream from the ICR III site on the (+) strand remained the same in the presence or absence of PcrA. However, the second resistance point at the end of ICR III on the (+) strand became much stronger in the presence of PcrA. Even after 15 min digestion in the presence of PcrA the ExoIII was halted at the end of ICR III and could not progress into the rest of the *oriD*. These data indicate that when PcrA is recruited the ternary complex reorganizes somewhat differently than the binary RepD–*oriD* complex forming strong contacts at the end boundary of ICR III and outside the core *oriD* ~74–80 bp upstream from the ICR I site (Figure 9).

DNaseI footprinting experiments with supercoiled pCERoriD revealed footprints of RepD on the (+) and (−) strands within *oriD*, consistent with binding of RepD

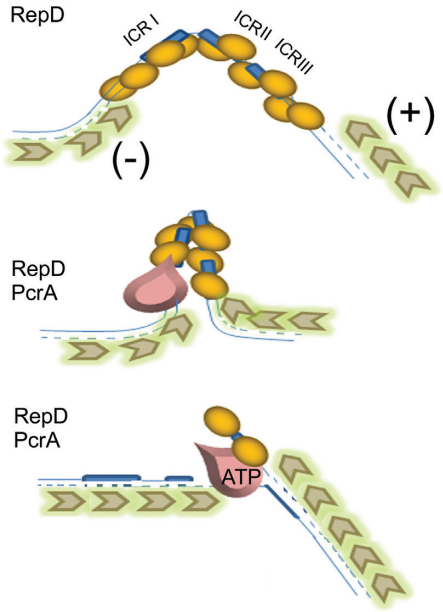

Figure 9. RepD-mediated PcrA recruitment at *oriD*. A speculative schematic model to summarize the combined footprint data and explain the molecular events associated with RepD-mediated recruitment of PcrA at *oriD*. The top panel shows an open-loose RepD-*oriD* complex that protects the DNA from ExoIII digestion upstream and downstream from *oriD*. The precise architecture of this complex is not known. The apparent stoichiometries are based upon our combined footprinting and AUC data but should be considered with caution. At high ExoIII concentrations and prolonged digestions of the (−) strand, ExoIII can pass through ICR I but stops in the first half of ICR II. In the opposite direction on the (+) strand, at high concentrations and prolonged digestions the ExoIII can pass with difficulty through ICR III into ICR II and then into ICR I where it stops. The middle panel shows that PcrA is recruited upstream of the ICR I site and the PcrA–RepD–*oriD* ternary complex contracts into a closed more compact conformation. Even at high concentrations and prolonged digestions, ExoIII cannot pass through the upstream PcrA-recruitment site on the (−) strand. It also fails to pass through the ICR III site in the opposite direction on the (+) strand. The bottom panel shows the ADPNP-induced rearrangement of the ternary complex. As a consequence of ADPNP (non-hydrolysable analogue of ATP)-binding to PcrA the complex rearranges further with ExoIII on the (−) strand easily passing through the PcrA upstream recruitment site and through the ICR I site to stop within the first half of ICR II. From the opposite direction on the (+) strand, ExoIII can now pass through the ICR III and ICR II sites but stops at the ICR I site. These rearrangements are consistent with an ATP-induced movement of PcrA from the RepD dimer bound to ICR I to the RepD dimer bound to ICR II to set up a translocation competent RepD–PcrA complex.

molecules in the ICR I-III sites. However, an additional DNaseI hypersensitive site appeared to form at 55–61 bp upstream from ICR I site on the (+) strand when RepD was bound to *oriD*. In the presence of RepD and PcrA, this DNaseI hypersensitive site disappeared, whilst two other hypersensitive sites appeared nearby in the region extending further upstream 62–90 bp from ICR I. This is consistent with a reorganization of the binary RepD-DNA complex when PcrA is also bound. The area where these effects were observed coincided broadly with the ExoIII resistance point 74–80 bp upstream from the ICR I site. The combined data reinforce the notion that initial RepD binding to *oriD* forms an extended loose complex that recruits PcrA upstream from the ICR I site (Figure 9).

ATP binding induces re-modelling of the PcrA–RepD–*oriD* ternary complex

Upon binding of ATP by PcrA the ternary complex changes drastically, as indicated by the differences in the ExoIII footprinting patterns in the presence and absence of ADPNP. On the (−) strand as the ExoIII approached the ICR I site, the upstream resistance point outside the *oriD* and the second resistant point at the front of ICR I disappeared, whereas the resistance point within the first half of ICR II strengthened. Similar changes were also apparent at the other end of *oriD* on the (+) strand as the ExoIII approached the ICR III. In the presence of ADPNP, the resistance point at the end of ICR III weakened and ExoIII progressed beyond ICR III into ICR II. The effect of ATP binding on the ternary complex was also detected by gel shift assays. In the presence of ADPNP or ADP, the initial extended ternary complex was reduced. The combined data indicate that ATP binding by PcrA induces remodelling of the ternary complex, perhaps setting up PcrA to start the translocation process upon ATP hydrolysis (Figure 9).

Subtle rearrangements have also been observed within the replication origin of the filamentous phage f1. Progressive binding of the replication initiator protein gpII at the three repeated sequences β, γ and δ produces an extended complex that bends and locally melts the DNA for nicking to occur (28). The PcrA–RepD–*oriD* system may be organized in an analogous manner through progressive binding of RepD, PcrA and ATP to set up a complex competent for processive unwinding. In our model for RepD-mediated loading of PcrA at *oriD* we propose that there is an ATP-induced hand-over event of PcrA from the RepD dimer bound to ICR I, which presumably initially recruits PcrA, to the RepD dimer bound to ICR II (Figure 9). This is consistent with the loss of the ExoIII resistance point within ICR I and the strengthening of the resistance point within ICR II observed in the presence of ADPNP (Figure 1). Our ExoIII footprinting and gel shift experiments cannot confirm unequivocally that PcrA remains bound in a ternary complex in the presence of ADPNP or ADP. Our data are equally consistent with a scenario whereby PcrA dissociates from the ternary complex in the presence of nucleotides. However, this is an unlikely scenario since RepD and PcrA have been shown to remain associated in a processive tight active complex coupling ATP hydrolysis to DNA unwinding (10,12,29). Further evidence, albeit indirect, that PcrA is still associated with the ternary complex is offered by our DNaseI footprinting of the (+) strand shown in Figure 4B. The DNaseI footprinting patterns of the ternary complex in the presence and absence of ADPNP are identical and different than that of RepD alone. If PcrA were to dissociate from the complex in the presence of ADPNP then one would expect the DNaseI footprinting patterns of the ternary complex in the presence and absence of ADPNP to be different, which is not the case. Therefore, PcrA must

remain bound in the complex even in the presence of ADPNP or ADP.

Recruitment of PcrA by RepD results in a visible change in DNA conformation

The model proposed above is consistent with our AFM imaging data. AFM images of protein–DNA complexes fell in two categories depending on the severity of the protein induced bend (sharp or shallow). It is possible that wild-type RepD may nick at *oriD* but religate the DNA during the course of sample preparation, resulting in a mixed population of nicked and religated DNA. For this reason, the RepD mutant R189K was also studied, as it is severely compromised with respect to DNA religation and thus yields a population of nicked DNA covalently attached to *oriD*. As both population types were observed for both Rep proteins, we conclude that they do not correspond to separate populations of nicked and religated DNA.

When PcrA was incubated with RepD and R189K, the proportion of sharply bent DNA fragments increased significantly in comparison with DNA bound to Rep proteins alone, and the contour lengths of those sharply bent fragments were slightly less than their shallow-angled counterparts. Bending of the closely related RepC–*oriC* system has been documented before (26), however this is the first time that further induced bending by the recruitment of the PcrA helicase has been shown. The contraction in contour length of the sharply bent DNA suggests a rearrangement of *oriD*, with possibly a looping of the DNA around the RepD–PcrA complex. When ADPNP was added, the sharply bent protein–DNA complex was further rearranged, and the increased distribution of bend angles suggests a more flexible DNA molecule in this remodelled complex.

Different functions of the ICR I–III sites

Sequence comparisons of several contiguous plasmid replication origins revealed that sequence conservation is highest in ICR II and in ICR I, whilst ICR III exhibited the greatest sequence diversity (7). Such sequence conservation patterns may be indicative of a functional division of labour between the three ICR sites. ICR III confers specificity on the Rep–*ori* interaction resulting in plasmid specific replication *in vivo* (7). ICR II is highly conserved as it is the site of the cleavage reaction and participates in the termination of replication (6,7,30,31). ICR I is also well conserved in terms of sequence and our data suggest that its role is to participate in the initial recruitment of the host helicase at the plasmid *ori*. Overall we conclude that RepD-mediated recruitment of PcrA at *oriD* is a three step process. Initially, an extended RepD–*oriD* complex includes a region upstream from the core *oriD*. PcrA is recruited to this upstream region and finally upon ATP-binding PcrA relocates within the core *oriD*.

SUPPLEMENTARY DATA

Supplementary Data are available at NAR Online.

FUNDING

Biotechnology Biological Sciences Research Council (BBSRC) grant (BB/E004717/1 to P.S.); Doctoral Training Award from BBSRC to the Astbury Centre (BB/D526502/1 to G.P.L.); University of Leeds (to N.H.T.); the Aviv fluorescence optics for the analytical ultracentrifuge was provided by a BBSRC equipment grant (BBF0111561 to D.J.S.). Funding for open access charge: Biotechnology Biological Sciences Research Council.

Conflict of interest statement. None declared.

REFERENCES

1. Gillespie,M.T. and Skurray,R.A. (1988) Structural relationships among chloramphenicol-resistance plasmids of *Staphylococcus aureus*. *FEMS Microbiol. Lett.*, **51**, 205–210.
2. Daini,O.A. and Akano,S.A. (2009) Plasmid-mediated antibiotic resistance in *Staphylococcus aureus* from patients and non-patients. *Sci. Res. Essay*, **4**, 346–350.
3. Del Solar,G., Giraldo,R., Ruiz-Echevarria,M.J., Espinosa,M. and Diaz-Orejas,R. (1998) Replication and control of circular bacterial plasmids. *Microbiol. Mol. Biol. Rev.*, **62**, 434–464.
4. Khan,S.A. (2000) Plasmid rolling-circle replication: recent developments. *Mol. Microbiol.*, **37**, 477–484.
5. Novick,R.P. (1989) Staphylococcal plasmids and their replication. *Ann. Rev. Microbiol.*, **43**, 537–565.
6. Koepsel,R.R., Murray,R.W., Rosenblum,W.D. and Khan,S.A. (1985) The replication initiator protein of plasmid pT181 has sequence-specific endonuclease and topoisomerase-like activities. *Proc. Natl Acad. Sci. USA*, **82**, 6845–6849.
7. Thomas,C.D., Balson,D.F. and Shaw,W.V. (1990) *In vitro* studies of the initiation of staphylococcal plasmid replication. Specificity of RepD for its origin (*oriD*), and characterization of the Rep-ori tyrosyl ester intermediate. *J. Biol. Chem.*, **265**, 5519–5530.
8. Zock,J.M., Birch,P. and Khan,S.A. (1990) Specificity of RepC protein in plasmid pT181 DNA replication. *J. Biol. Chem.*, **265**, 3484–3488.
9. Khan,S.A. (2005) Plasmid rolling-circle replication: highlights of two decades of research. *Plasmid*, **53**, 126–136.
10. Zhang,W., Dillingham,M.S., Thomas,C.D., Allen,S., Roberts,C.J. and Soultanas,P. (2007) Directional loading and stimulation of PcrA helicase by the replication initiator protein RepD. *J. Mol. Biol.*, **371**, 336–348.
11. Soultanas,P., Dillingham,M.S., Papadopoulos,F., Phillips,S.E.V., Thomas,C.D. and Wigley,D.B. (1999) Plasmid replication initiator protein RepD increases the processivity of PcrA DNA helicase. *Nucleic Acids Res.*, **27**, 1421–1428.
12. Slatter,A.F., Thomas,C.D. and Webb,M.R. (2009) PcrA helicase tightly couples ATP hydrolysis to unwinding double-stranded DNA, modulated by the initiator protein for plasmid replication, RepD. *Biochem.*, **48**, 6326–6334.
13. Petit,M.A., Dervyn,E., Rose,M., Entian,K.D., McGovern,S.D., Ehrlich,S.D. and Bruand,C. (1998) PcrA is an essential DNA helicase of *Bacillus subtilis* fulfilling functions both in repair and rolling-circle replication. *Mol. Microbiol.*, **29**, 261–273.
14. Petit,M.A. and Ehrlich,S.D. (2002) Essential bacterial helicases that counteract the toxicity of recombination proteins. *EMBO J.*, **21**, 3137–3147.
15. Iordanescu,S. and Bargonetti,J. (1989) *Staphylococcus aureus* chromosomal mutations that decrease efficiency of Rep utilization in replication of pT181 and related plasmids. *J. Bacteriol.*, **171**, 4501–4503.
16. Iordanescu,S. and Basheer,R. (1991) The *Staphylococcus aureus* mutation *pcrA3* leads to the accumulation of pT181 replication initiation complexes. *J. Mol. Biol.*, **221**, 1183–1189.
17. Iordanescu,S. (1993) Plasmid pT181-linked suppressors of the *Staphylococcus aureus pcrA3* chromosomal mutation. *J. Bacteriol.*, **175**, 3916–3917.

18. Iordanescu,S. (1993) Characterization of the Staphylococcus aureus chromosomal gene *pcrA*, identified by mutations affecting plasmid pT181 replication. *Mol. Gen. Genet.*, **241**, 185–192.
19. Chang,T.-L., Naqvi,A., Anand,S.P., Kramer,G., Munshi,R. and Khan,S.A. (2002) Biochemical characterization of the *Staphylococcus aureus* PcrA helicase and its role in plasmid rolling circle replication. *J. Biol. Chem.*, **277**, 45880–45886.
20. Anand,S.P., Mitra,P., Naqvi,A. and Khan,S.A. (2004) *Bacillus anthracis* and *Bacillus cereus* PcrA helicases can support DNA unwinding and *in vitro* rolling-circle replication of plasmid pT181 of *Staphylococcus aureus*. *J. Bacteriol.*, **186**, 2195–2199.
21. Ruiz-Masó,J.A., Anand,S.P., Espinosa,M., Khan,S.A. and del Solar,G. (2006) Genetic and biochemical characterization of the *Streptococcus pneumoniae* PcrA helicase and its role in plasmid rolling circle replication. *J. Bacteriol.*, **188**, 7416–425.
22. Caryl,J.A. and Thomas,C.D. (2006) Investigating the basis of substrate recognition in the pC221 relaxosome. *Mol. Microbiol.*, **60**, 1302–1218.
23. Streeter,S.D., Papapanagiotou,I., McGeehan,J.E. and Kneale,G.G. (2004) DNA footprinting and biophysical characterization of the controller protein C.Ahdl suggests the basis of a genetic switch. *Nucleic Acids Res.*, **32**, 6445–6453.
24. Metzger,W. and Heumann,H. (1994) Footprinting with Exonuclease III. *Methods Mol. Biol.*, **30**, 11–20.
25. Schuck,P. (2000) Size distribution analysis of macromolecules by sedimentation velocity ultracentrifugation and Lamm equation modeling. *Biophys. J.*, **78**, 1606–1619.
26. Koepsel,R.R. and Khan,S.A. (1986) Static and initiator protein-enhanced bending of DNA at a replication origin. *Science*, **233**, 1316–1318.
27. Thomas,C.D., Nikiforov,T.T., Connolly,B.A. and Shaw,W.V. (1995) Determination of sequence specificity between a plasmid replication initiator protein and the origin of replication. *J. Mol. Biol*, **254**, 381–391.
28. Higashitani,A., Greenstein,D., Hirokawa,H., Asano,S. and Horiuchi,K. (1994) Multiple DNA conformational changes induced by an initiator protein precede the nicking reaction in a rolling circle replication origin. *J. Mol. Biol.*, **237**, 388–400.
29. Toseland,C., Martinez-Senac,M.M., Slatter,A.F. and Webb,M.R. (2009) The ATPase cycle of PcrA helicase and its coupling to translocation on DNA. *J. Mol. Biol.*, **392**, 1020–1032.
30. Iordanescu,S. and Projan,S.J. (1988) Replication termination for staphylococcal plasmids: plasmids pT181 and pC221 cross-react in the termination process. *J. Bacteriol.*, **170**, 3427–3434.
31. Murray,R.W., Koepsel,R.R. and Khan,S.A. (1989) Synthesis of single-stranded plasmid pT181 DNA *in vitro*: initiation and termination of DNA replication. *J. Biol. Chem.*, **264**, 1051–1057.